

Key Points:

- The GFDL X-SHiELD global storm-resolving model can explicitly represent rotating convection worldwide
- Cyclonically rotating updrafts predominate over the oceans and higher latitudes, less so over land and in the deep tropics
- Environmental controls explain much of the predominance of cyclonic updrafts but internal storm dynamics are also important

Supporting Information:

Supporting Information may be found in the online version of this article.

Correspondence to:

L. Harris,
lucas.harris@noaa.gov

Citation:

Harris, L., Zhou, L., Kaltenbaugh, A., Clark, S., Cheng, K.-Y., & Bretherton, C. (2023). A global survey of rotating convective updrafts in the GFDL X-SHiELD 2021 global storm resolving model. *Journal of Geophysical Research: Atmospheres*, 128, e2022JD037823. <https://doi.org/10.1029/2022JD037823>






Received 7 SEP 2022

Accepted 24 APR 2023

Author Contributions:

Conceptualization: Lucas Harris
Data curation: Linjiong Zhou, Alex Kaltenbaugh, Kai-Yuan Cheng
Formal analysis: Lucas Harris
Funding acquisition: Lucas Harris
Investigation: Linjiong Zhou, Alex Kaltenbaugh, Kai-Yuan Cheng, Chris Bretherton
Methodology: Lucas Harris, Linjiong Zhou, Kai-Yuan Cheng
Software: Linjiong Zhou, Alex Kaltenbaugh, Spencer Clark
Supervision: Lucas Harris
Validation: Lucas Harris, Alex Kaltenbaugh, Spencer Clark
Writing – original draft: Lucas Harris
Writing – review & editing: Spencer Clark, Kai-Yuan Cheng, Chris Bretherton

A Global Survey of Rotating Convective Updrafts in the GFDL X-SHiELD 2021 Global Storm Resolving Model

Lucas Harris¹ , Linjiong Zhou² , Alex Kaltenbaugh^{1,3}, Spencer Clark^{1,4} , Kai-Yuan Cheng² , and Chris Bretherton^{4,5} 

¹NOAA/Geophysical Fluid Dynamics Laboratory, Princeton, NJ, USA, ²Cooperative Institute for Modeling Earth Systems, and Program on Atmospheric and Oceanic Sciences, Princeton University, Princeton, NJ, USA, ³University Corporation for Atmospheric Research, Boulder, CO, USA, ⁴Allen Institute for Artificial Intelligence, Seattle, WA, USA, ⁵Department of Atmospheric Sciences, University of Washington, Seattle, WA, USA

Abstract We present the global characteristics of rotating convective updrafts in the 2021 version of GFDL's eXperimental System for High-resolution prediction on Earth-to-Local Domains (X-SHiELD), a kilometer-scale global storm resolving model (GSRM). Rotation is quantified using 2–5 km Updraft Helicity (UH) in a year-long integration forced by analyzed SSTs. Updrafts with UH magnitudes above 50 m² s⁻² are common over the mid-latitude continents, where they are associated with severe weather especially in the warm seasons but are also common over most tropical ocean basins. In nearly all areas cyclonically rotating convection dominates, with larger UH values increasingly preferring cyclonic rotation. The ratio of cyclonic to anticyclonic updrafts is largest in the subtropical and mid-latitude oceans and is slightly lower over mid-latitude continents. The ratio of cyclonic to anticyclonic updrafts can be substantively explained by the mean storm-relative helicity (SRH) in convective regions, indicating the importance for environmental controls on the sense of storm rotation, although internal storm dynamics also plays a role in the generation of anticyclonic updrafts.

Plain Language Summary Thunderstorm updrafts are sometimes observed to rotate. This rotation is important especially in severe thunderstorms and developing hurricanes since it allows an updraft to last longer and become more intense. However, little is known about rotating updrafts outside of these isolated contexts and there is not yet a global survey of this phenomenon. We have developed a new model called X-SHiELD, which is one of an emerging class of atmosphere computer models that can represent individual thunderstorm updrafts worldwide. This means it can simulate rotating updrafts, unlike traditional global models, and can do so globally, unlike regional models for forecasting thunderstorms. We find that rotating thunderstorms are common in many warmer places in the world, even if they are not always as strong as the fearsome severe thunderstorms in the central US. In the northern hemisphere, counter-clockwise rotating storms are most common, although clockwise-rotating storms are also produced by the model in lesser numbers. In the southern hemisphere, the opposite is true. The most common direction of thunderstorm rotation is primarily governed by large-scale weather systems, not directly by the earth's rotation. Specific behavior of individual thunderstorms also controls which way they rotate.

1. Introduction

Thunderstorm updrafts are sometimes observed to rotate. This is well-understood in the context of severe weather in continental convection, especially over the contiguous United States (CONUS), for example, Kain et al. (2008). More recently the role of vortical hot towers (VHTs; Guimond et al., 2010; Hendricks et al., 2004) in tropical cyclone intensity changes has become better understood. But updraft rotation is typically studied in isolated events, and it has not been considered as a broadly distributed phenomenon. This is in part due to the lack of observations of rotating convection. Indeed, the frequency of strongly rotating updrafts—especially mesocyclones—even in the CONUS was poorly understood before the installation of a dense nationwide Doppler radar network, as seen through the increases in radar-detected tornadoes after 1990 (Verbout et al., 2006) and improved understanding that most mesocyclones are not associated with tornadoes (Trapp et al., 2005). The spatial distribution of rotating updrafts has been scarcely studied except as for its role in creating severe weather, specifically supercell thunderstorms, mesoscale convective systems (MCSs), and tornadoes. Rotation of sub-severe storms—those not meeting National Weather Service severe weather criteria—has apparently not been studied

at all. VHTs are beginning to be observed through geostationary satellites and in some aircraft observations (Hogsett & Stewart, 2014) but most effort at understanding these uses regional simulations, and exclusively in the context of mature and intensifying tropical cyclones where there has been some effort to better understand their role in genesis and intensification (Kilroy, 2021, and references therein; Wang, 2018; Zawislak, 2020, and references therein; Hendricks et al., 2004). An appreciation for rotating updrafts elsewhere is virtually absent. Current global models used for routine weather and climate simulation are too coarse to represent updrafts or their rotation. Regional convective-scale models focus on severe weather and VHTs, and run at most only for a few days, restricting understanding of the patterns of their occurrence, and of interactions between successive days' events or between scales.

Updraft rotation, even if not of severe magnitude, is worth studying as it may provide useful insight into the characteristics of thunderstorms, including their life cycles, mutual interactions, and their dependence upon the larger-scale environment. This would hold true worldwide, not just for mid-latitude severe convection or VHTs, but also for air-mass convection, convective clusters, tropical cyclogenesis, and tropical continental convection. As convective-scale regional models extend their forecasts into the medium range and global models approach convection-allowing scales, a better understanding of the behavior of explicit convection and its interactions with larger scales becomes increasingly important. This is especially true as convective parameterizations are weakened or disabled in these models, requiring an accurate simulation of multi-day and upscale impacts of explicit convection to properly maintain and predict synoptic and global circulations.

Emerging global storm-resolving models (GSRMs; Satoh et al., 2019) are ideally suited to give a global picture of rotating convection and its interactions with the large-scale environment. Previous research (Cheng et al., 2022; Miyamoto et al., 2013; Seiki et al., 2022; Wedi et al., 2020; and references therein) has made some progress on understanding the properties of global explicit convection but not of rotating convection cells.

In this paper we investigate rotating convection in a year-long GSRM simulation, forced by analyzed sea-surface temperatures, of the GFDL System for High-resolution prediction on Earth-to-Local Domains (SHIELD). This configuration has been submitted to Phase 2 of the Dynamics of the Atmospheric general circulation Modeled On Non-hydrostatic Domains initiative (DYAMOND; <https://www.esiwace.eu/services/dyiamond-initiative/services-dyiamond-winter>, Stephan et al., 2022). We will find that convection frequently rotates, and that the preferred sense of rotation depends on latitude and on geography, especially over continents. We will also find that environmental shear provides a good estimate for the prevalence of either sense of rotation, but that local storm-scale dynamics still play an important role in the development of rotation. This work is accomplished by taking concepts from severe weather research, developed principally over the CONUS, and applying them worldwide, in combination with analyses typically applied to intraseasonal and longer-timescale variability. Due to the variety of forms of convection worldwide and numerous potential sources of rotation in updrafts we only speculate on the processes generating storm-scale vorticity in this GSRM and save such investigation for future research.

Experimental aircraft developed by the National Aeronautics and Space Administration (NASA) are designated "X-Planes." SHIELD's dynamical core, FV3, was first developed at NASA (Lin & Rood, 1996; Putman & Lin, 2007), and FV3's creator Shian-Jiann Lin was trained as an aeronautical engineer. In honor of this heritage, we have named this GSRM "X-SHIELD," the eXperimental configuration of SHIELD.

2. Methods

X-SHIELD is a configuration of SHIELD (Harris et al., 2020). We briefly describe the 2021 version used in this paper. X-SHIELD is discretized on a C3072 (3.25 km) cubed-sphere grid with 79 vertical levels, with the lowest mid-level at 10 m above the surface. X-SHIELD couples the nonhydrostatic FV3 dynamical core to physical parameterizations including GFDL microphysics, version 2 (Zhou et al., 2019, 2022), the prognostic TKE form of the EDMF turbulence scheme (Han & Bretherton, 2019), and the Noah-MP land-surface model with high-resolution fixed files provided by the Environmental Modeling Center. X-SHIELD also uses Scale-Aware SAS (Han et al., 2016) to parameterize shallow convection; there is no deep convective parameterization. There are no interactive aerosols, and the only chemistry is stratospheric ozone, represented by a simple linear parameterization based on the observed long-term climatology.

X-SHIELD grew out of an earlier GFDL FV3-based GSRM, which was submitted to the first phase of DYAMOND (Stevens et al., 2019) and has been part of earlier evaluations (Judt et al., 2021; Nugent et al., 2022; Turbeville

et al., 2022). A 40-day simulation with the 2021 version of X-SHiELD was submitted to the second phase of DYAMOND (Duras et al., 2021) and evaluation is underway (Stephan et al., 2022).

We perform a 15-month integration starting at 00 UTC on 20 October 2019 and ending 00 UTC on 17 January 2021 (455 days), although only dates in 2020 are considered in this manuscript. We use a mixed-layer ocean to compute sea-surface temperature (SST); as per the DYAMOND protocol the SSTs are nudged toward analyzed ECMWF SSTs. A complementary analysis of this simulation and a companion warmed-climate simulation is described in Cheng et al. (2022).

Convective frequencies are computed using native-resolution output of 6-hr column-maximum updraft velocity (W_{up}) below 100 hPa, and 6-hr extreme values of counter-clockwise (positive) and clockwise (negative) 2–5 km updraft helicity (UH). We define “intense” convection as that for which W_{up} is greater than 10 m s^{-1} . We define

$$\text{UH} = \int_{2 \text{ km}}^{5 \text{ km}} w \zeta \, dz, \quad (1)$$

where w is the vertical velocity and ζ is the relative vertical vorticity. For example, for a 2–5 km mean w of 10 m s^{-1} and a corresponding ζ of 10^{-3} s^{-1} , UH would be $30 \text{ m}^2 \text{ s}^{-2}$. This quantity is a frequently used proxy for severe weather in convective-scale prediction models (Droegemeier et al., 1993; Kain et al., 2008). Typically, thresholds of $50\text{--}250 \text{ m}^2 \text{ s}^{-2}$ are used to indicate potentially severe weather events, but this threshold is notably model- and resolution-dependent (Kain et al., 2008). In FV3, both vertical velocity and vertical vorticity are grid-cell mean quantities (the latter computed exactly using Stokes' theorem; Lin & Rood, 1997) and so UH can be computed exactly, leading to larger values in FV3-based models than those using other dynamical cores (Potvin et al., 2019). The threshold used by the Storm Prediction Center to indicate CONUS severe weather in FV3-based convective-scale models is $250 \text{ m}^2 \text{ s}^{-2}$, corresponding to the 99.85 percentile of hourly maximum UH values during the peak of severe weather season in May (about 1 out of 650 grid columns; see <https://www.spc.noaa.gov/exper/href>). These high UH values are very rare worldwide, as we will see below. Note that the maximum vertical velocity in a deep, intense updraft will be attained in the upper troposphere, well above the 2–5 km layer in which UH is computed. Thus, in deep updrafts W_{up} is usually much larger than the vertical velocity that is used to compute UH. While 2–5 km UH is designed for mid-latitude warm-season severe convection and may not be the best way to characterize rotation in all convective events—cf. the use of potential vorticity by Rogers (2010) for VHTs—it still is a useful, simple, and broadly applicable metric for detecting rotation in a wide array of convective events, as we will see below.

Counts of W_{up} and UH are the number of columns in each 0.75×0.75 -degree bin (roughly equal to the 80-km grid bins used for validation of severe storm forecasts; cf. Hitchens et al., 2013; Sobash et al., 2011) in which the 6-hr maximum exceeds given threshold values. Counts are normalized by the number of cells in a bin, so the values are the number of times per season/year any given model column can expect a threshold event. Counts are of individual grid columns and not convective objects. Analysis is restricted to areas below 60° latitude in both hemispheres, poleward of which convection is rare.

3. Results

3.1. Global Distribution of Intense and Rotating Convection

The global distribution and annual cycle of deep convection is well documented (Houze et al., 2015; Liu et al., 2007). We see in Figure 1 that intense convection in X-SHiELD (defined as $W_{\text{up}} > 10 \text{ m s}^{-1}$) is most common over the deep tropics year-round and follows the migration of the ITCZ. Intense convection is also present in the extratropical storm tracks and in common tropical cyclone paths, and in the South Pacific Convergence Zone. We also see frequent intense convection in the warm seasons over mid-latitude continents, most notably over the central United States but also in northern Eurasia, central China, Argentina, southern Africa, and Australia. Over large areas in the subtropics, especially in the southern hemisphere, intense convection is absent. Intense convection is also nearly absent over the ocean poleward of 40° latitude. These results are in line with the observed frequency of convection as defined from satellite-based radar reflectivity (Houze et al., 2015; Liu et al., 2007) and give confidence that X-SHiELD is producing a realistic frequency of convection. The quantitative comparison to observed precipitation and convective parameters in the following subsection also shows that X-SHiELD is producing a realistic simulation of convection more generally.

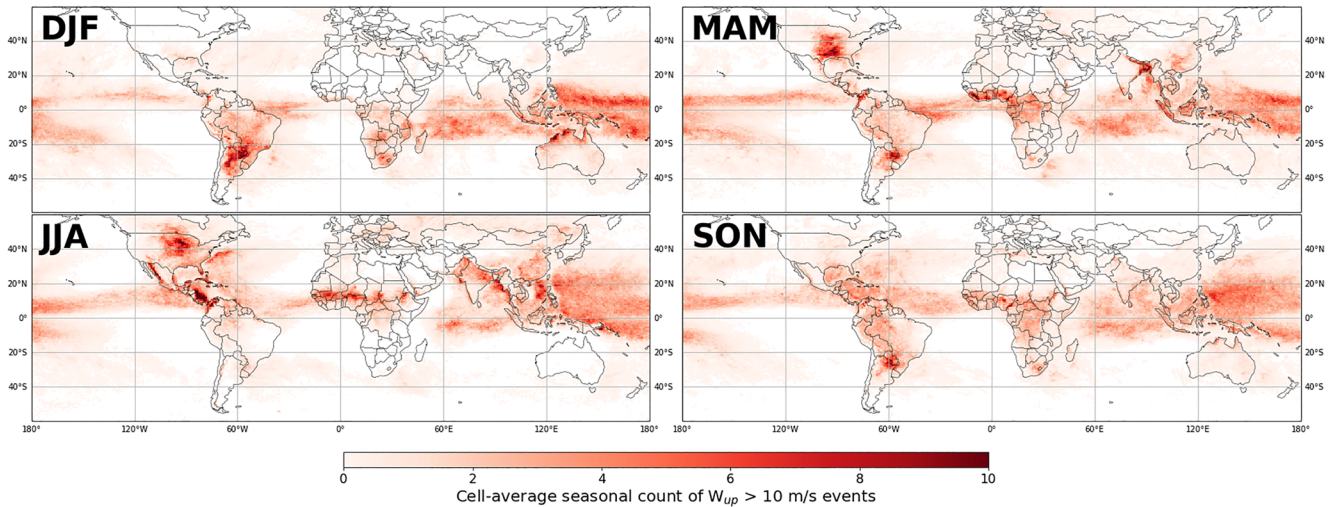


Figure 1. Seasonal 0.75-by-0.75-degree bin-mean count of intense convection events ($W_{up} > 10 \text{ m s}^{-1}$). This and successive figures represent the number of 6-hourly intervals per season for which any grid column in a particular bin can expect to have intense convection. White represents bins with no events in a season.

The spatial distribution of rotating updrafts largely follows that of convective updrafts, although the sense of rotation shows a more complex pattern. Figure 2 shows the frequency of UH magnitudes greater than $50 \text{ m}^2 \text{ s}^{-2}$ for both positive (counter-clockwise) and negative (clockwise) values. This threshold is much smaller than traditional thresholds used for CONUS severe weather prediction but is useful for detecting storm rotation in lower latitudes where environmental sources of vertical vorticity are weak (see Figures 7 and 15 below).

Cyclonic UH (positive in the northern hemisphere, negative in the southern hemisphere) dominates away from the equator, especially over the ocean; this signature is weaker over the continents. We quantify this in Figure 3: yellow regions correspond to areas in which cyclonic updrafts are at least four times as frequent as anticyclonic, while purple indicates a closer equality of the two orientations. Anticyclonic updrafts predominate only in small regions along the equator, where "cyclonic" has little meaning; along the peaks of mountain ranges, where local effects may prefer one sign of rotation; and in some areas of very few convective events. In the high northern latitudes cyclonic updrafts are several times more frequent than anticyclonic, although this represents a small number of events.

Except in the deep tropics, oceanic convection is preferentially cyclonically rotating. In continental convective hot spots cyclonic updrafts still tend to be more frequent, but there are also significant numbers of anticyclonic updrafts. This correspondence is by no means universal and there are interesting geographic and seasonal variations seen in Figure 2, such as a greater preference for cyclonic rotation in the Gulf of Mexico and Southeastern US. The seasonal cycle of this ratio over the Indian Subcontinent is also unusual: in the monsoon season (JJA) and into SON the convection is more oceanic in nature, with a distinct cyclonic preference, but in MAM there is no such preference.

How frequently do intense updrafts rotate? Figure 4 shows the fraction of $W_{up} > 10 \text{ m s}^{-1}$ updrafts that meet the $50 \text{ m}^2 \text{ s}^{-2}$ UH criterion, in either sense of rotation. While not all updrafts rotate to an appreciable degree, in nearly all convective regions some significant fraction (at least 10%) do. In general, rotation is more frequent in the subtropics and mid-latitudes, where about half of all intense updrafts also meet this UH threshold. Except for the Himalayas where intense convection is common (Houze et al., 2007; Romatschke et al., 2010) the apparent high frequency of rotating convection in mountainous regions is likely due to a very small sample of events. This is most noticeable in the Cascades and Andes ranges. Caution must be used in interpreting the results in steeply mountainous regions.

For UH values meeting the severe threshold ($250 \text{ m}^2 \text{ s}^{-2}$) many of these features are even more clear (Figure 5). Positive severe UH dominates in the northern hemisphere and negative severe UH dominates in the southern hemisphere. As we expect, most severe UH events occur over land, and the few events occurring over the ocean are overwhelmingly cyclonic. Larger counts of severe UH correspond to the warm seasons of the CONUS,

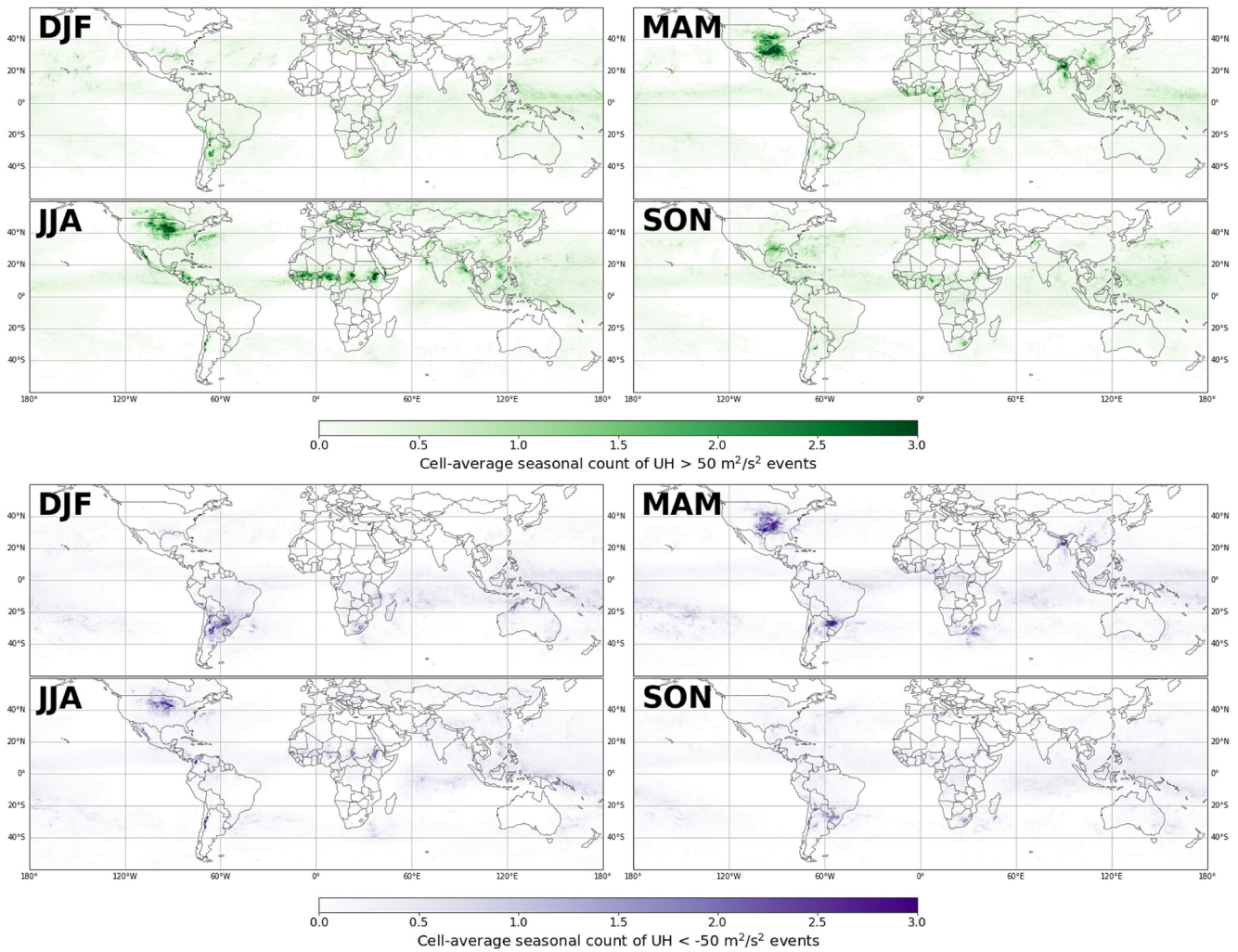


Figure 2. As in Figure 1, except for Updraft Helicity magnitudes larger than 50 m² s⁻²: top, positive (counter-clockwise rotating) events; bottom, negative (clockwise-rotating) events.

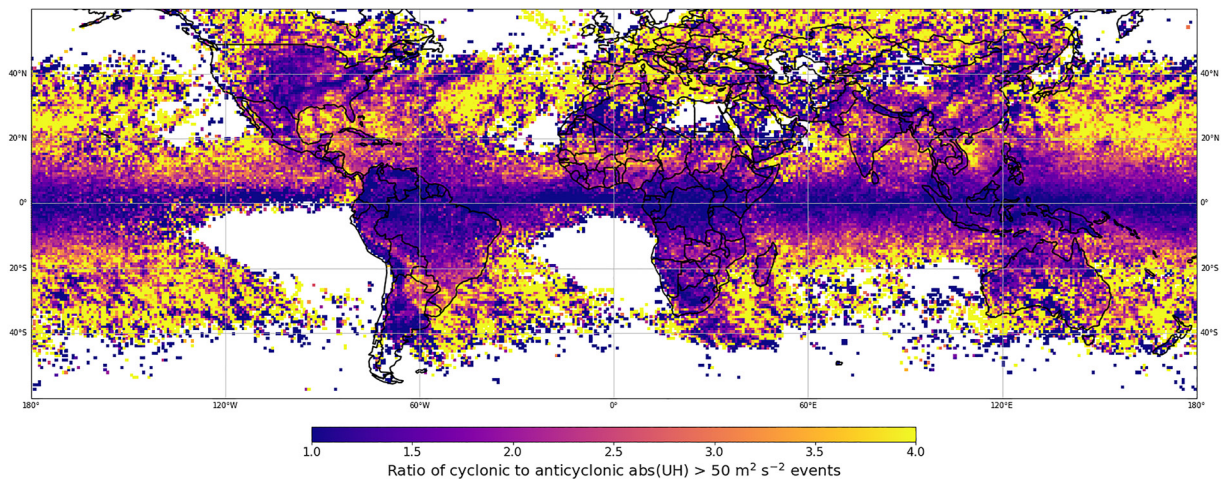


Figure 3. Annual ratio of cyclonic to anticyclonic Updraft Helicity events of magnitude >50 m² s⁻². White regions represent areas where no UH events of this magnitude occurred.

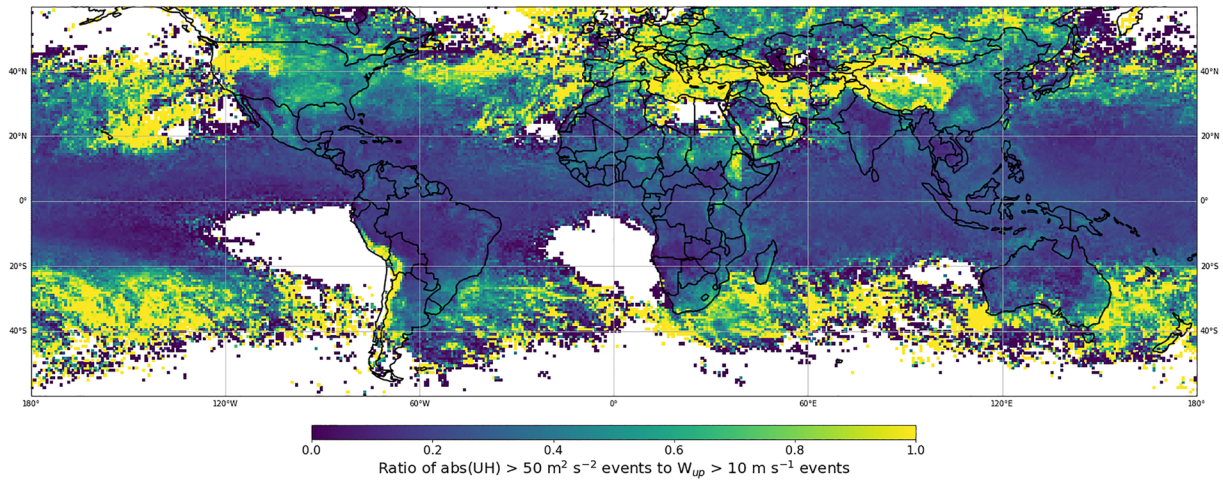


Figure 4. Annual fraction of intense updrafts which rotate (ratio of abs (Updraft Helicity) > 50 m² s⁻² to W_{up} > 10 m s⁻¹).

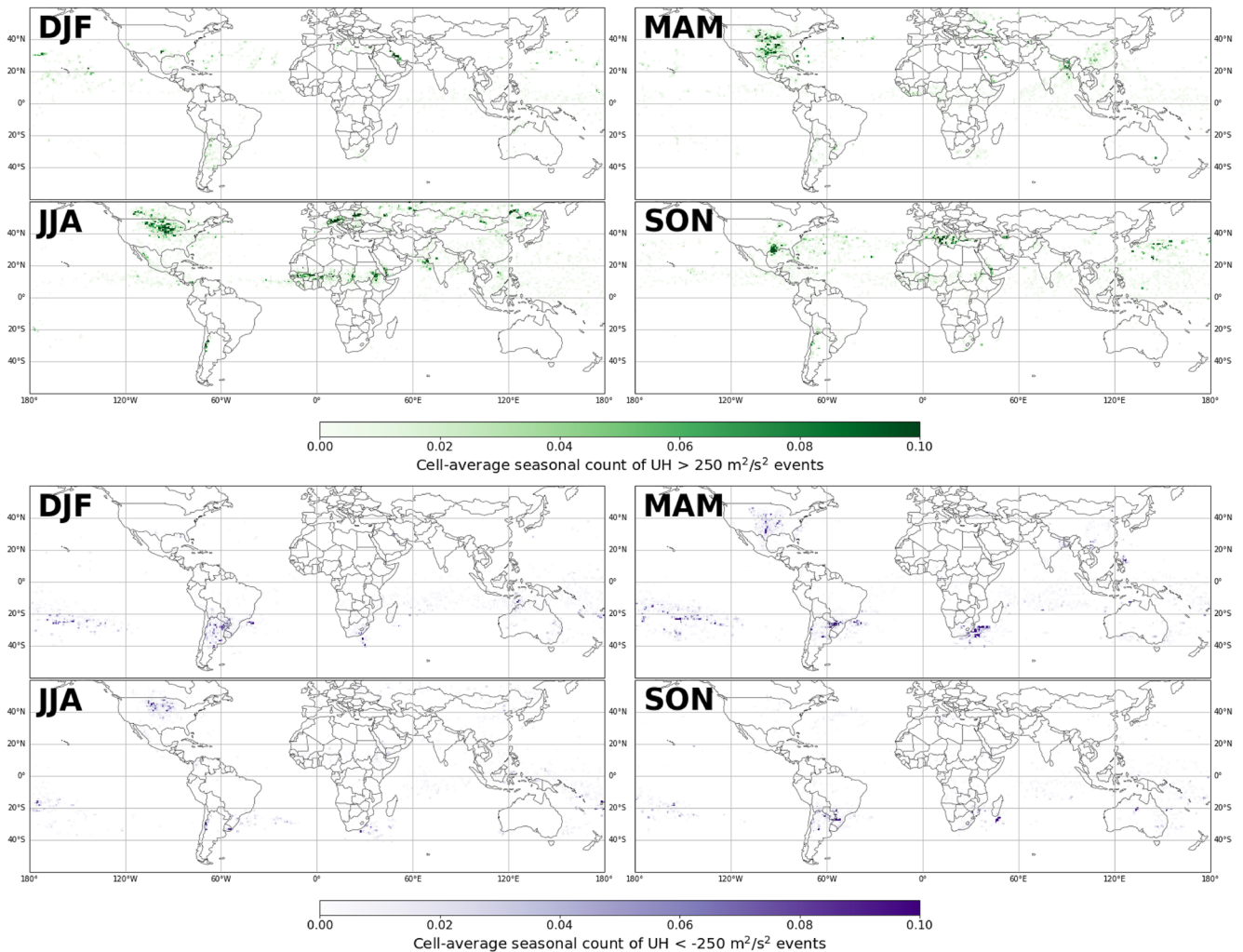


Figure 5. As in Figure 2, but for a 250 m² s⁻² threshold. Note the smaller upper bound for the colorbar compared to Figure 2.

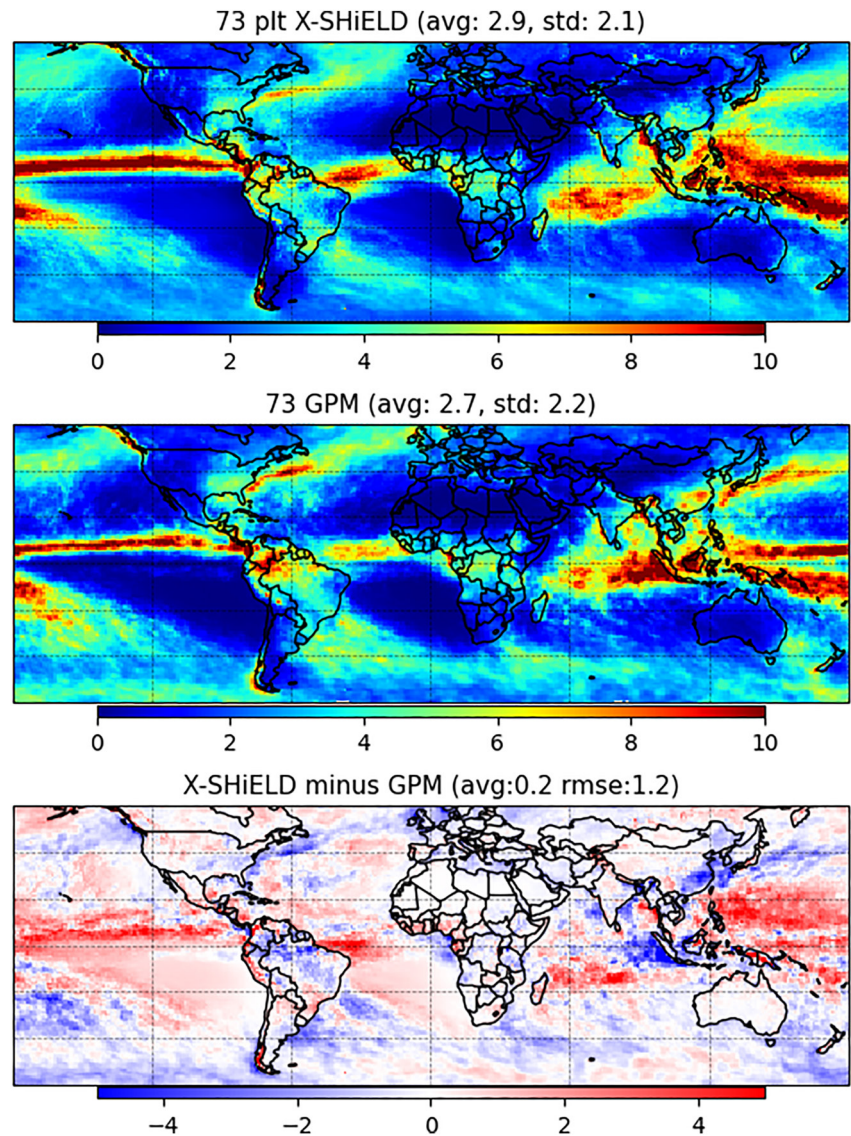


Figure 6. Year-mean precipitation (mm d^{-1}) in X-SHiELD compared to the Global Precipitation Measurement observation for 2020. Numbers in panel titles represent the average (“avg”), standard deviation (“std”) and root-mean square error (“rmse”) for the Global Precipitation Measurement satellite (GPM) domain of 60°S – 60°N latitude.

Argentina, South Africa, sub-Saharan Africa, the Bay of Bengal, and in a band from central Europe into eastern Siberia. Figure 5 shows that anticyclonic updrafts of this high magnitude are rare, especially over the ocean, and in the locations where they occur at all (CONUS, Bay of Bengal, South America) they are still much less common than cyclonic severe updrafts.

3.2. Validation of Convection and Rotation

Precipitation helps validate how well the model represents deep convection globally. X-SHiELD well reproduces 2020’s observed precipitation from the Global Precipitation Measurement satellite (GPM; Huffman et al., 2019) with global root mean square errors (RMSE) of only about 1.2 mm/day (Figure 6). This compares well with CMIP6 climate models (cf., Boucher et al., 2020; Zhao et al., 2018), despite X-SHiELD only having a single year’s simulation to be validated. X-SHiELD has a global average precipitation of 2.9 mm/day compared to the GPM estimate of 2.7 mm/day, although observational and reanalysis datasets disagree on the global average precipitation rate and the precise value remains elusive (Gehne et al., 2016). X-SHiELD tends to have too

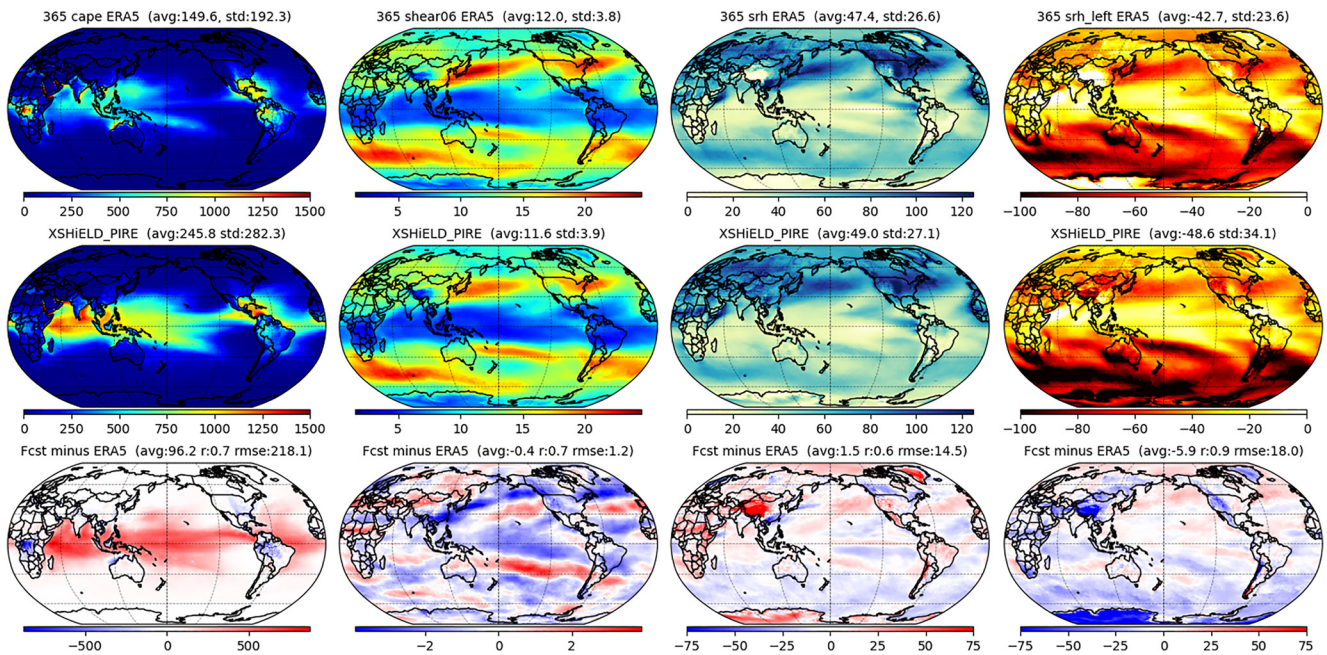


Figure 7. Year-mean convective parameters in X-SHiELD compared to ERA5 (top row) for 2020. Columns are, from left to right, convective available potential energy (CAPE), 0–6 km shear, Right- storm-relative helicity (SRH), and Left-SRH. See text for discussion of CAPE between ERA5 and X-SHiELD. Numbers in panel titles follow those of Figure 6, with the addition of "r" for pattern correlation.

much precipitation in the tropical convective regions and too little in the extratropical storm tracks. Areas of lighter precipitation are also broader than in GPM, possibly due to an excess of shallow convective precipitation in X-SHiELD.

We can also validate simulated convective parameters against a reanalysis to evaluate the ability of X-SHiELD to simulate convection and convective organization. Figure 7 compares year-mean simulated convective available potential energy (CAPE), 0–6 km shear, and both senses of storm relative helicity (SRH, described in Section 3.5) to the ECMWF ReAnalysis version 5 (ERA5; Hersbach et al., 2020). The shear and SRH shows broad agreement with the reanalysis, with largest errors over high terrain in Tibet, Greenland, and Antarctica where there is little convection. There is a clear difference in the magnitudes of CAPE between X-SHiELD and ERA5, especially over the warm equatorial oceans, although the spatial patterns are similar and the pattern correlation is 0.7. This may be explained by the differences between X-SHiELD and the model used to create ERA5. While X-SHiELD explicitly simulates deep convection, ERA5's Integrated Forecast System uses a convective parameterization with a CAPE closure (Bechtold et al., 2014) to trigger convection. An examination of the instantaneous fields (not shown) finds that CAPE is longer lived in X-SHiELD than in ERA5, representing the slower consumption of CAPE in the absence of a convective parameterization. Similar results for CAPE in explicit- and parameterized-convection simulations were found by Becker et al. (2021) over tropical Africa.

Worldwide observations of rotating convection do not exist. Over the CONUS simulated UH values above a certain threshold are considered proxies for severe weather and so severe weather reports (tornadoes, strong winds, large hail) are used as a validation data set (cf., Hitchens et al., 2013; Sobash et al., 2011). Here, we take 2020 tornado reports from the Storm Events Database (<https://www.ncdc.noaa.gov/stormevents/>) and following this methodology (henceforth "Sobash-SPC methodology"), sort daily events into 0.75-by-0.75° bins. Under this methodology, a "hit" is when there is at least one event—either a simulated UH magnitude over the threshold or a tornado report—within a bin in a day. The resulting grid is then smoothed using a Gaussian filter with a one-bin (0.75°) radius to preserve smaller-scale features in the UH fields. The Sobash-SPC methodology is an imperfect way of comparing models to storm reports: there is not a direct mapping between simulated storm rotation and a real-world tornado report, and only about 1 in 4 mesocyclones (intense rotating thunderstorms) produce tornadoes (Trapp et al., 2005). Storm reports are also notably an imperfect means for forecast validation (Herman et al., 2018) and the "bin" methodology can weight single events as heavily as a localized outbreak. Keeping these

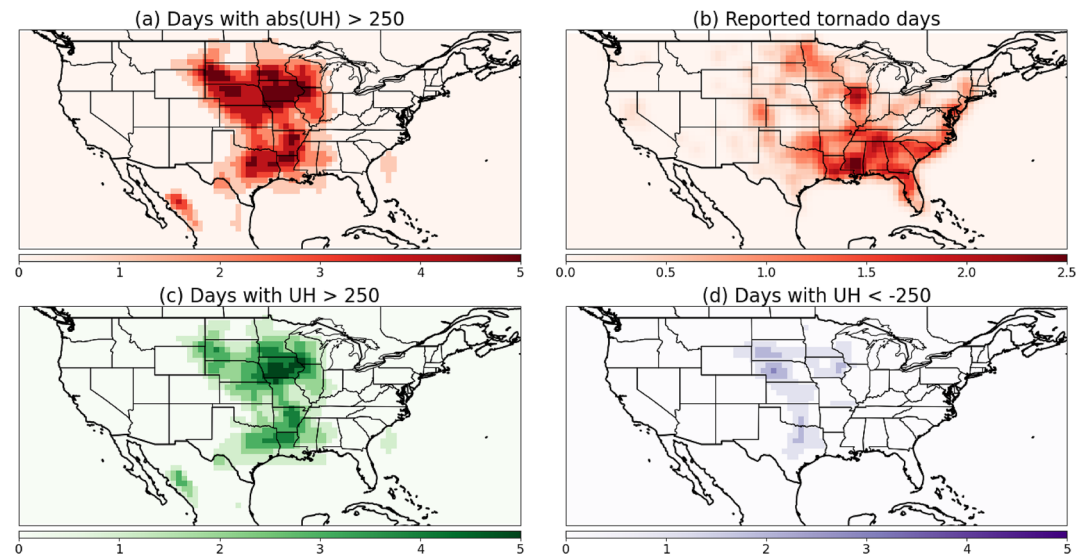


Figure 8. Contiguous United States (CONUS) number of days with severe Updraft Helicity or a reported tornado in 2020. See text for methodology. The colorbar for observed tornado days in (b) differs from the others reflecting the small fraction of rotating storms that cause tornadoes (Trapp et al., 2005).

caveats in mind, the Sobash-SPC methodology is still useful for our purposes given its prior application to model validation (cf., Potvin et al., 2019).

There is a similarity in the pattern of severe rotation days (Figure 8a, both senses of rotation) and reported tornado days (Figure 8b). The two maxima seen in the UH frequencies, one centered over Iowa, the other over Louisiana and Texas, separated by a local minimum from central Oklahoma into Illinois, bears a striking although likely coincidental resemblance to the pattern of tornado reports in 2020, with maxima in northern Illinois and in southern Mississippi. This result gives us some confidence that X-SHiELD is simulating the annual frequency of high-threshold UH reasonably well, given the limitations of our one year of simulation and its less-than-optimal compatibility with the available validation data set. However, the observed higher frequency of tornadoes in the Southeastern US, along the front range of the Rocky Mountains, and along the US Atlantic Coast, is not reflected in the simulated UH frequency. X-SHiELD also produces significant counts of severe rotation days in the high northern Plains, especially in sparsely populated western Nebraska and South Dakota, not present in the storm reports. It is also evident from the bottom two panels of Figure 8 again that while cyclonic (positive) UH predominates, anticyclonic UH is not uncommon especially in the upper midwestern states.

3.3. Quantification of Global Convection and Rotation

Figure 9 shows the ratios of the zonal mean frequencies of positive versus negative UH exceeding different threshold values, for the ocean and separately for the continents in both the western and eastern hemispheres. The zonal means validate the qualitative patterns deduced from Figure 2: over the ocean cyclonic rotation dominates and increases poleward until about 20–30° latitude. This corresponds to regions in which tropical cyclogenesis is common, which are virtually all cyclonic. An example of tropical cyclone related UH is given in Figure S1 in the Supporting Information S1, in which cyclonic helicity dominates in the eyewall although updrafts of both senses of directions are seen in convective cells embedded in the outer rainbands. Over the land the pattern is more complex, as this monotonic increase is only seen in the deep tropics equatorward of 10° latitude, with local minima in the ratio in the mid latitudes corresponding to convective hot spots: the central US and Argentina in the western hemisphere, and in west Africa, South Africa, Australia, and across central Eurasia in the eastern hemisphere. Since the continental hot spots all lie at different latitudes, we separate the zonal-mean analysis by hemisphere to avoid averaging out the latitudinal variation.

Nearly universally the ratios between cyclonic and anticyclonic UH increase with increasing threshold. These relations hold all the way up to 200 m² s⁻², nearing the model's threshold for severe weather. At this 200 m² s⁻²

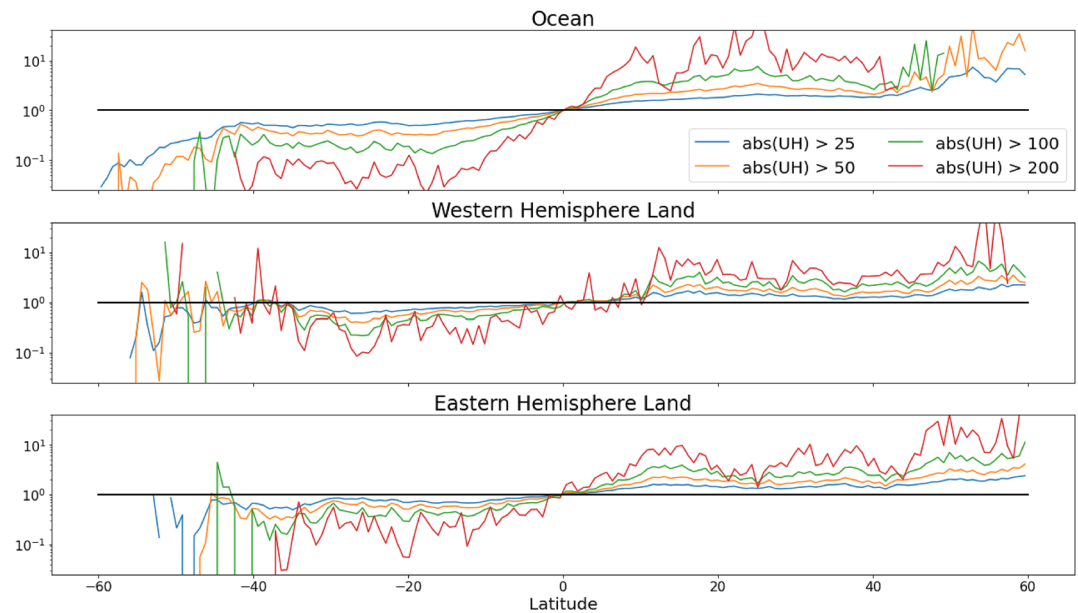


Figure 9. Zonal-mean annual relative counts of positive to negative Updraft Helicity events of different magnitudes over the ocean (top), western-hemisphere land (WH: North and South America, middle), and eastern-hemisphere land (EH: Africa, Eurasia, Australia, and Maritime Continent, bottom). Count ratios in each 0.75° latitude band are plotted on a log scale. Figure S2 in the Supporting Information S1 shows absolute counts of both senses of rotation.

magnitude the relationships become even more striking, notwithstanding the additional noisiness in the plot due to the relatively small number of events (Figure S2 in the Supporting Information S1).

Continental hot spots show a smaller but still distinct preference for cyclonically rotating updrafts. This is especially true for strong storms with UH thresholds of $200 \text{ m}^2 \text{ s}^{-2}$, for which cyclonically rotating updrafts are 3–5 times more frequent than anticyclonic updrafts. This is in line with the typical CONUS experience that severe storms are most frequently cyclonically rotating, as was also seen in X-SHIELD for a $250 \text{ m}^2 \text{ s}^{-2}$ threshold in Figure 5. This is exemplified by a summertime Mesoscale Convective System (MCS) event in the northern Midwestern US (Figure S3). In both the earlier (west) and later (east) phases of the MCS's life cycle, cellular convection dominates and both signs of UH are seen, although cyclonic UH dominates. In the mature (central) phase of the MCS, some embedded cells are seen but there is a broad area of updrafts and cyclonic UH with very little anticyclonic UH. This may suggest broader uplift in a rotationally sheared environment, such as along a squall line.

We plot probability distribution functions (PDFs) of the UH in Figure 10 in regions and latitude bands to better quantify the relative frequencies of each sense of rotation. Here we show only UH for intense convection, so that the results are not dominated by weak updrafts. Over the ocean in both hemispheres there is a greater preference for cyclonic UH that increases in more poleward latitudes and with UH threshold; there are also more total events counted at lower latitudes over the ocean. The PDFs over land are more complex: cyclonic UH is not as clearly dominant and the increasing prevalence of UH at higher latitudes is not monotonic as it is over the ocean. However, the same broad pattern is seen. Intriguingly, nearly all the curves meet at a certain crossover point, about $25 \text{ m}^2 \text{ s}^{-2}$. This may indicate that $25 \text{ m}^2 \text{ s}^{-2}$ constitutes a UH “noise floor” of weak rotating updrafts, at which point the frequencies of either sense of rotation are so similar it becomes difficult or impossible to distinguish the two signs. This level of UH would correspond to a quite weak mesocyclone: a $25 \text{ m}^2 \text{ s}^{-2}$ UH updraft with a mean vertical velocity of 5 m s^{-2} in the 2–5 km layer would have a mean vorticity of only $1.7 \times 10^{-3} \text{ s}^{-1}$, well below the minimum threshold for mesocyclone detection (Trapp et al., 2005). Alternately, this could be attained by a strong localized vorticity without an updraft: for vorticity of 10^{-2} s^{-1} then this UH threshold would be reached for vertical velocities less than 1 m s^{-1} .

We can deduce some facts about the origins of rotation in convective updrafts from these ratios. Since the timescale of individual convective updrafts is short, we cannot ascribe their sense of rotation directly to the convergence

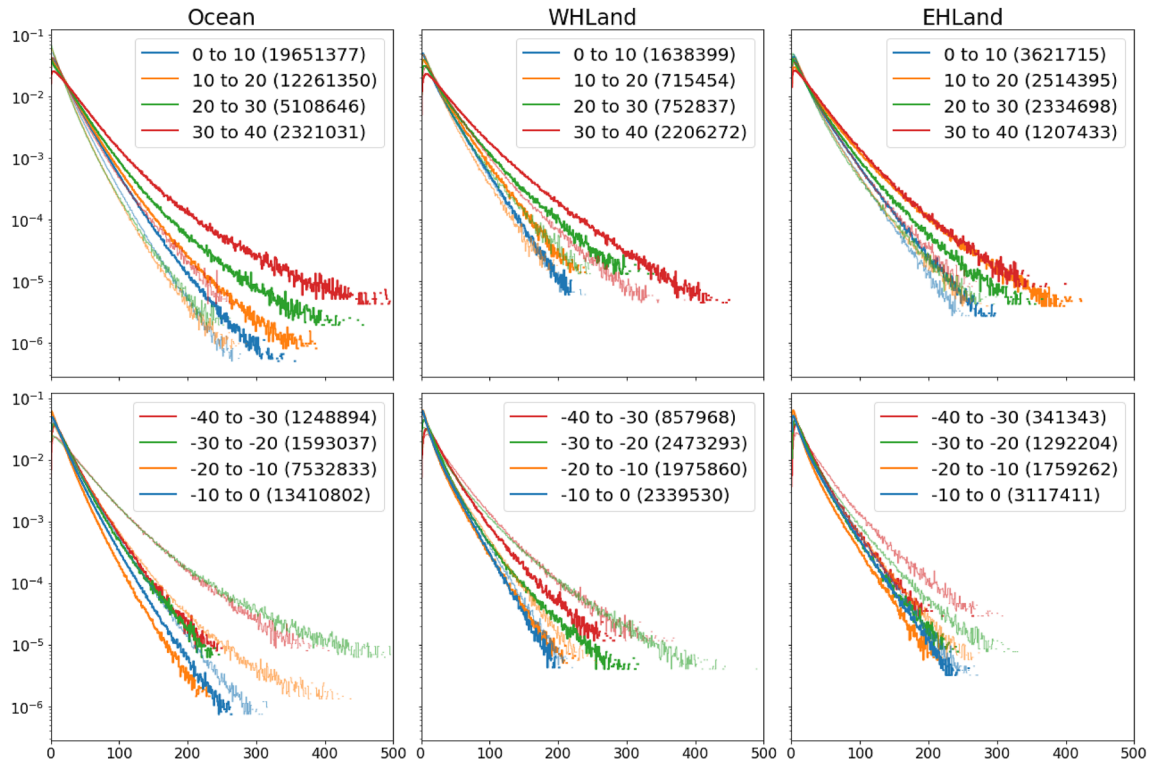


Figure 10. Conditional probability distribution functions of positive (heavy lines) and negative (light, thin lines) Updraft Helicity (UH) for intense convection (grid cells in which $W_{up} > 10 \text{ m s}^{-1}$) in different regions (as in Figure 9) and latitude bands. Top row shows northern hemisphere latitudes, bottom row shows southern hemisphere latitudes. Normalization is by the number of cells with intense convection, given in parentheses in the legends. UH bins with fewer than 10 events are not plotted.

of planetary vorticity, although this has an indirect effect on convection through synoptic-scale systems that give preference to one sign of rotation or the creation of horizontal shear zones that affect updrafts. This inference does not rule out the convergence of relative vorticity as a contributor to rotating updrafts.

3.4. Example: Rotating Convection in the Tropical Western Pacific

We now show concrete examples of rotating convection events, on the synoptic scale and on individual convective cells. The JJA tropical Pacific provides an illustration of these processes (Figure 11). In both the deep tropics and subtropics, rotating updrafts are associated with westward-propagating convective events (indicated by low OLR values). In the subtropics (20–30°N) cyclonic updrafts are usually several times more frequent than anticyclonic updrafts, although we find at this threshold ($50 \text{ m}^2 \text{ s}^{-2}$) that the events with the most frequent cyclonic updrafts are co-located with significant numbers of anticyclonic updrafts. In these events the ratio is much closer to unity (and in some cases anticyclonic rotation dominates) than in the events for which fewer rotating updrafts are present. An analysis with a larger $100 \text{ m}^2 \text{ s}^{-2}$ threshold (Figure S4 in the Supporting Information S1) however reveals that stronger rotation is cyclonically dominated, with only a small number of events in which strong anticyclonic rotation dominates. This gives an indication that significant numbers of updrafts with both senses of rotation are created, but that the anticyclonically rotating updrafts are weaker. We will return to this point below. Meanwhile, in the deep tropics (0–10°N) there are roughly equal numbers of both signs of UH.

These suppositions are supported by computing the PDFs for just this region and these months (Figure 12, left). The frequency of cyclonic updrafts is roughly the same for all thresholds in the deep tropics and over 10 to 20°N latitude, with slightly less in the subtropics. The frequency of anticyclonic updrafts clearly decreases in the more poleward bands, and the frequency relative to the number of cyclonic updrafts decreases with threshold, to the point that in the subtropics, an appreciable number of $UH > 150 \text{ m}^2 \text{ s}^{-2}$ updrafts are counted but $UH < -150 \text{ m}^2 \text{ s}^{-2}$ is very rare. Again, the crossover of the curves in both panels is at about $25 \text{ m}^2 \text{ s}^{-2}$, lending credence to our hypothesis that this is the noise floor for UH.

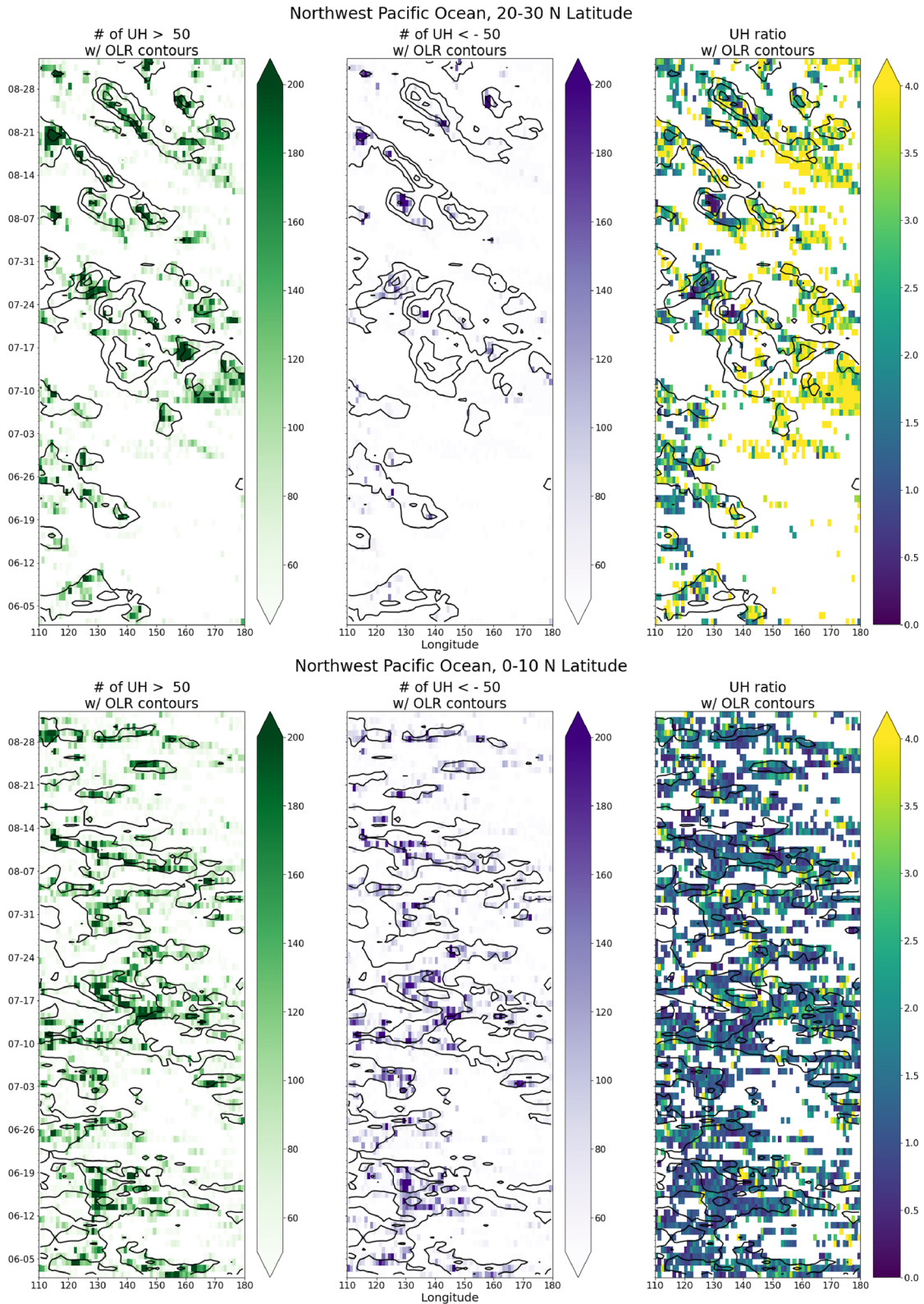


Figure 11. Hovmuller (time-longitude) plots averaged within two latitude bands in the Western Pacific for JJA. Shaded colors are counts in 1-degree longitude bins of daily Updraft Helicity (UH) $> 50 \text{ m}^2 \text{ s}^{-2}$ events for positive (left) and negative (center) UH values; the shading in the right panel is the ratio of positive to negative events. Only bins with at least 50 columns per day exceeding the UH thresholds are shown. Black contours represent $100\text{--}220 \text{ W m}^{-2}$ values of latitudinally-averaged outgoing longwave radiation with a 40 W m^{-2} contour interval.

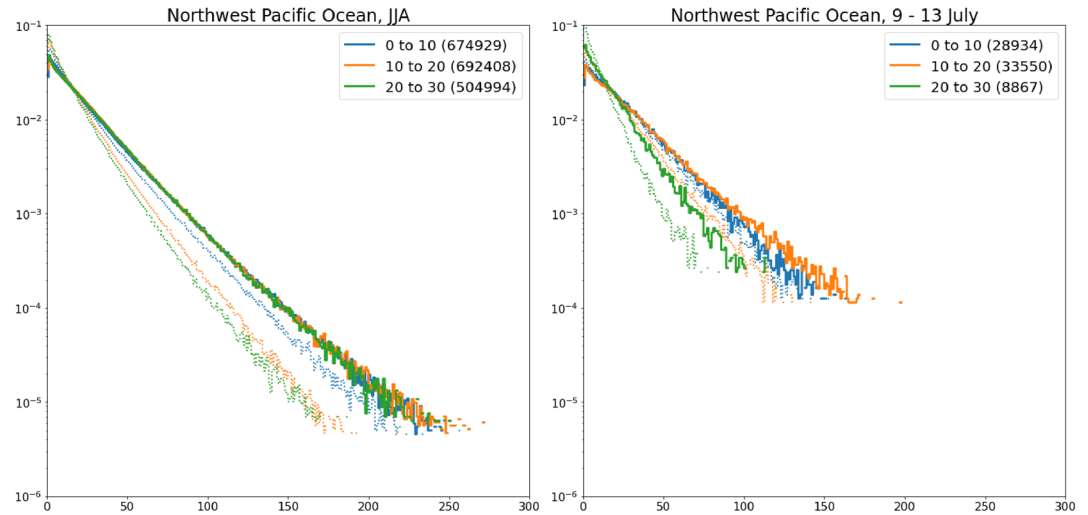


Figure 12. (left) Conditional probability distribution functions over latitude bands ($^{\circ}$ N) of Updraft Helicity (UH; $m^2 s^{-2}$, positive solid, negative dotted) in intense updrafts for the region and time period shown in Figure 11. (right) Same but for the region shown in Figure 13. Normalization is by the number of cells with intense convection. Numbers in parens are the count of total events with UH magnitude greater than $25 m^2 s^{-2}$. Bins with fewer than 10 events are not plotted.

The distinctly enhanced preference for cyclonic rotation in the subtropics suggests that there is an environmental control at work in the generation of rotating convection, even if for individual events local vorticity generation of both signs is still active. This is identifiable from an examination of two specific regions in the tropical north-western Pacific for a four-day period in July 2020 (Figure 13). In the northern region, positive UH dominates (green) and there is relatively less negative UH (purple). The numbers are nearly equal in the southeastern region. The storms in the South China Sea show a larger number of cyclonic events than anticyclonic ones, but not overwhelmingly so. This relation is quantified by the PDF in Figure 12 (right) which shows nearly equal frequencies of both senses of rotating updrafts up to about $125 m^2 s^{-2}$ in the deep tropics, but many more cyclonic updrafts at higher latitudes. Note that this period is dominated by the first of three larger westward-propagating events (Figure 11, top-right panel) starting in early July and each lasting about 2 weeks. In other times, there are large quiescent regions (especially in the subtropics) and so the PDFs of this region do not precisely match those for the full summer (Figure 12, left) or full year (Figure 10).

By zooming in on these areas (Figure 14) we can get a better sense of the behavior of convective cells. In the subtropical region (Figure 14, top) many updraft tracks (gray contours) are seen, many of which overlap over the 48-hr period and not all of which are associated with strong rotation. In many cases those that do rotate show pairs of positive and negative UH (green and purple contours, respectively). Pairs of simultaneous cyclonic and anticyclonic updrafts, and the short lengths and thus short lifetimes of most individual cells' tracks (usually less than 50 km, lasting a few hours) suggest that convergence of planetary rotation is not the principal mechanism creating vorticity in these cells. These pairs can be compared to vorticity dipoles seen in the idealized simulations of Kilroy and Smith (2015) which arose by the tilting of horizontal shear vorticity into the vertical. Note that in this region the prevailing flow is northerly as part of the synoptic-scale circulation, and so here the cyclonic right-moving cells are to the west of the anticyclonic left-moving cells.

While large ($UH > 100 m^2 s^{-2}$) values of both signs are present in the subtropical region, so that the circumstances leading to individual storm formation are important for the sense of rotation and how large the UH gets, it is apparent from Figure 14 (top) that positive UH dominates. A simple count of the number of columns (insets, Figure 14) with threshold values of UH confirms our visual inspection. As was seen in Figure 11, subtropical events with many rotating updrafts tend to have both senses of rotation present, although the cyclonically rotating updrafts have larger UH. This again suggests the action of the local vorticity generation creating counter-rotating updraft pairs, with the cyclonic sense of vorticity being preferred. In the lower-latitude region (Figure 14, bottom) pairs of counter-rotating cells are again seen, although the vorticity couplets are less well-organized, and much more negative UH is present than in the subtropical region. Since planetary vorticity is so small within 10 degrees of the equator, and the convective cell lifetime so short (a few hours at most), we can conclude that the preference for one sign of rotation is

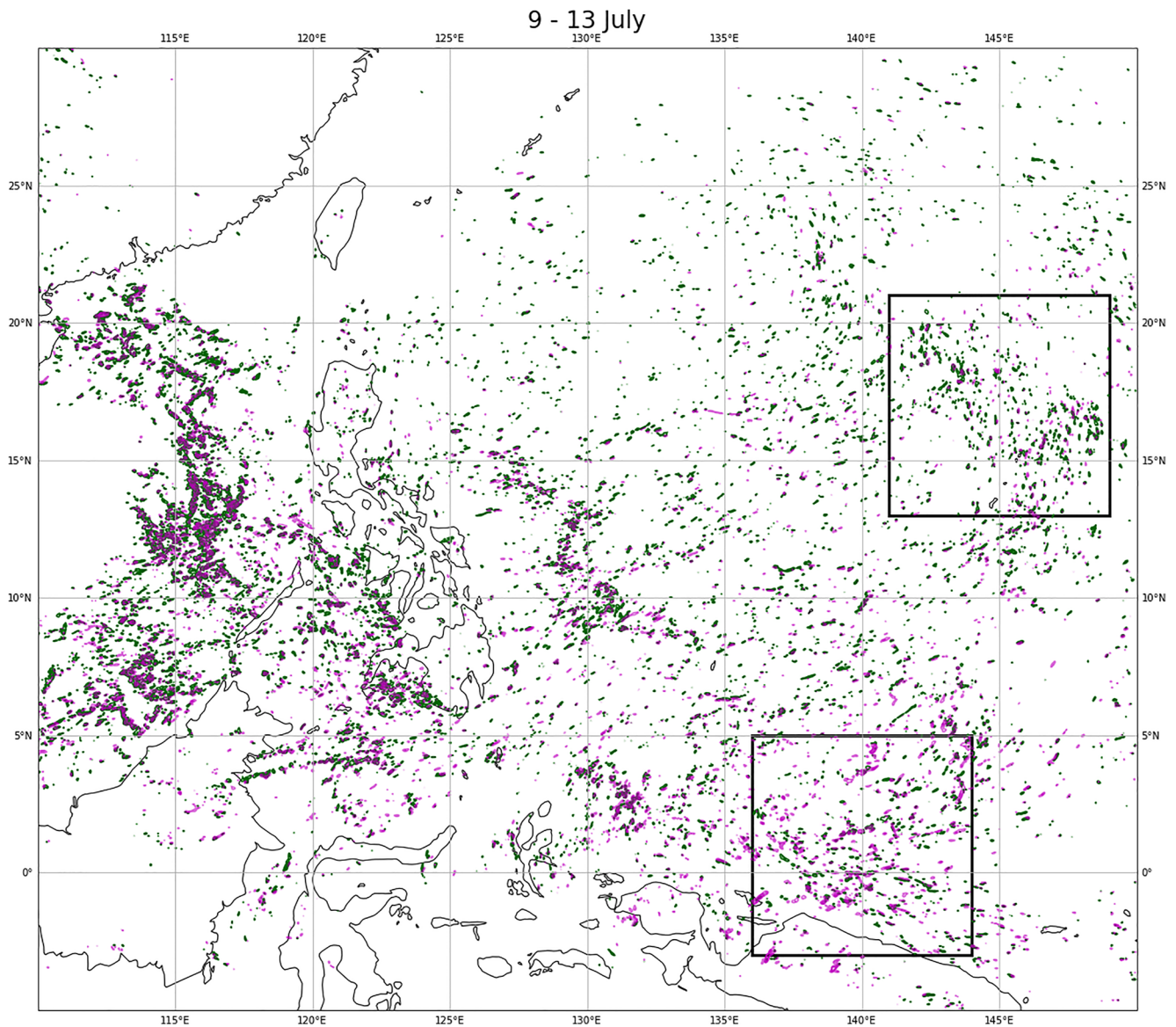


Figure 13. Period-extreme values of positive (green) and negative (purple) Updraft Helicity over the tropical Northwestern Pacific, over a 4-day period in July 2020. Contour interval is $50 \text{ m}^2 \text{ s}^{-2}$. Negative contours are semi-transparent and plotted over positive contours. Regions inside the boxes are shown in Figure 14.

principally influenced by the synoptic environment. Note that the existence of both senses of rotation and with a range of UH intensities implies that the rotating convection shown here is not merely the existence of an updraft stretching the environmental vorticity, but that there are processes at work which develop and amplify both signs of vorticity.

3.5. Role of Environmental Controls in Rotating Convection

We have suggested that the environmental vertical wind shear is an important if not the only factor in determining the ratios of cyclonic and anticyclonic updrafts. The role of Storm Relative Helicity (SRH) in creating rotating updrafts is well understood (Davies-Jones, 1984) and provides a useful means by which we can explain our results, independent of the geography, environment, and formation of the updrafts. SRH is the vertical integral (here 0–3 km above ground level) of the vector product of an estimated storm-relative wind and the vertical wind shear. Figure 15 shows yearly, zonal averages of 0–3 km SRH for the right- and left-moving storms, called R-SRH and L-SRH respectively using the definitions from Bunkers et al. (2000) and Bunkers (2002); the difference between the two senses is in the assumed storm motion, either right or left of the 0–6 km shear vector. The

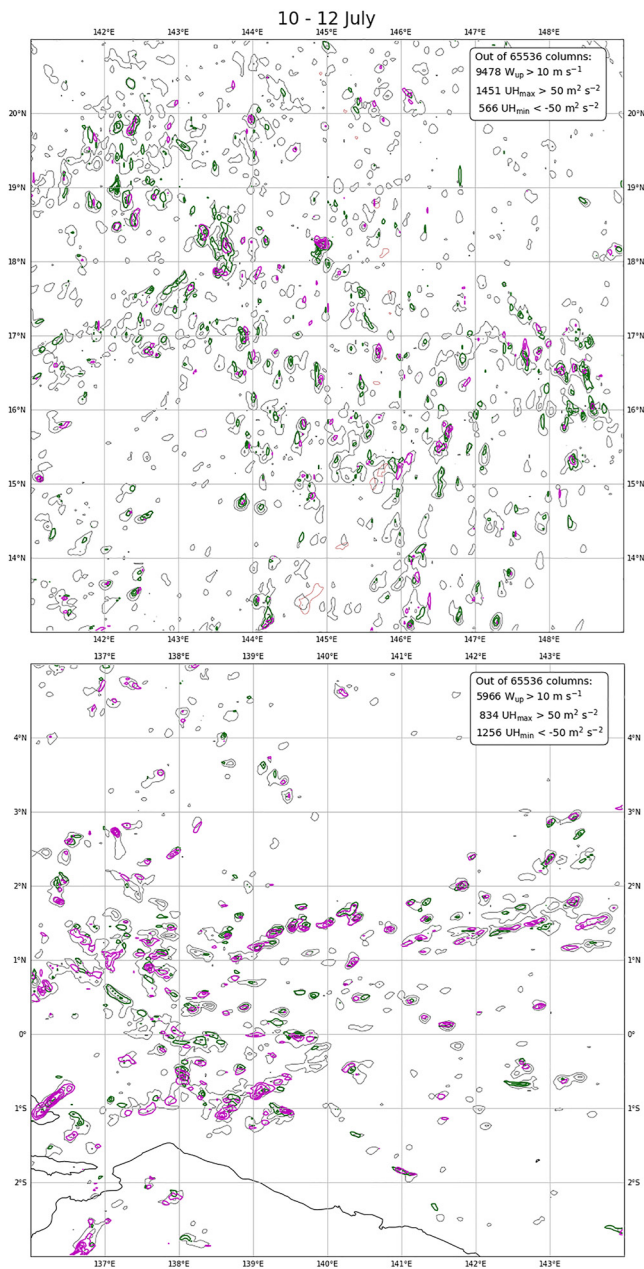


Figure 14. As in Figure 13 but zoomed-in over the subtropical (top) and deep tropical (bottom) convective regions and over a 2-day period. Gray contours are period-maximum W_{up} with a contour interval of 10 m s^{-1} . Text in boxes indicate the number of columns in each region meeting thresholds for W_{up} and both senses of Updraft Helicity anytime during this 2-day period.

precise calculation is given in Supporting Information S1 (Text S1). Here, we show both the mean weighted by counts of updrafts with max vertical velocity above 10 m s^{-1} , and the unweighted mean. The weighted mean removes the effects of intense cold-season mid-latitude cyclones—in which strongly deformational flows can create SRH values above $1000 \text{ m}^2 \text{ s}^{-2}$ —with little convection as well as quiescent periods also with little convective activity while emphasizing convective outbreaks. Here again, in the northern hemisphere we refer to R-SRH as cyclonic and L-SRH as anticyclonic, with the convention reversed in the southern hemisphere. The year-mean values of both senses of SRH (Figure 7, right two columns) matches well with the ERA5 reanalysis.

Figures 9 and 15 show a consistency between the SRH and the ratios of UH: the two senses of SRH are roughly equal at the equator and in the deep tropics, with the cyclonic sense becoming increasingly dominant steadily into the subtropics and mid-latitudes in both hemispheres. The difference in the means is modest in the subtropics and especially in the oceanic subtropics but should be sufficient to cause the simulated preference for cyclonic updrafts. There are large differences between the two orientations in the mid-latitude storm tracks and in land regions. Notably, Eastern Hemisphere continental SRH differences show a close match to the pattern of cyclonic updraft preference: maxima in the ratios toward cyclonic updrafts at 15 and 35°N , a minimum at 25°N , and an increase poleward of 30°S closely match similar maxima and minima in differences between cyclonic and anticyclonic SRH. In the continental Western Hemisphere, there is distinctly more cyclonic SRH poleward of 25° latitude, corresponding to the larger numbers of cyclonic updrafts in the mid-latitudes. This correspondence is not perfect: despite the distinct preference for cyclonic updrafts in the western hemisphere's continental subtropics, there is almost no difference between the two senses of SRH in the weighted-mean in this area.

Although the magnitude of the SRH difference in the mid-latitudes, especially over land, is significantly larger than the SRH difference over the subtropical oceans, this does not correspond to a larger preference for cyclonic updrafts. Indeed, over the subtropical oceans the preference for cyclonic updrafts is significantly larger than in the continental mid-latitudes, much more than can be expected from the SRH difference alone. This points to the well-recognized (cf., Emanuel, 1989) and fundamental distinction between tropical and mid-latitude convection, in which mid-latitude convection is typically longer-lived and more intense than that in the tropics and is supported by much larger CAPE and convective inhibition values. This more intense convection and its aggregation into mesoscale convective systems may create more storm-scale phenomena that can create and enhance both cyclonic and anticyclonic updrafts; Figure S3 in the Supporting Information S1, depicting such a system over the northern Midwest US, shows the possibility for these intense systems to create both senses of rotation. It is also possible that local geographic features over land can modify the preference for cyclonic updrafts.

Why does the ratio of cyclonic to anticyclonic storms increase with the threshold? We can speculate on the causes for this. It may be that stronger updrafts are able to tilt the environmental shear more strongly into vertical vorticity, which is more often cyclonic as seen by the preponderance of cyclonic SRH in most regions. It may also be true that flow convergence may locally enhance the SRH to high levels, thereby inducing rotation within developing updrafts. This is akin to the result of Nolan (2011) who found VHTs with strong rotation arising from local enhancement of SRH, or of Markowski et al. (1998) who deduced significant time and space variability in SRH.

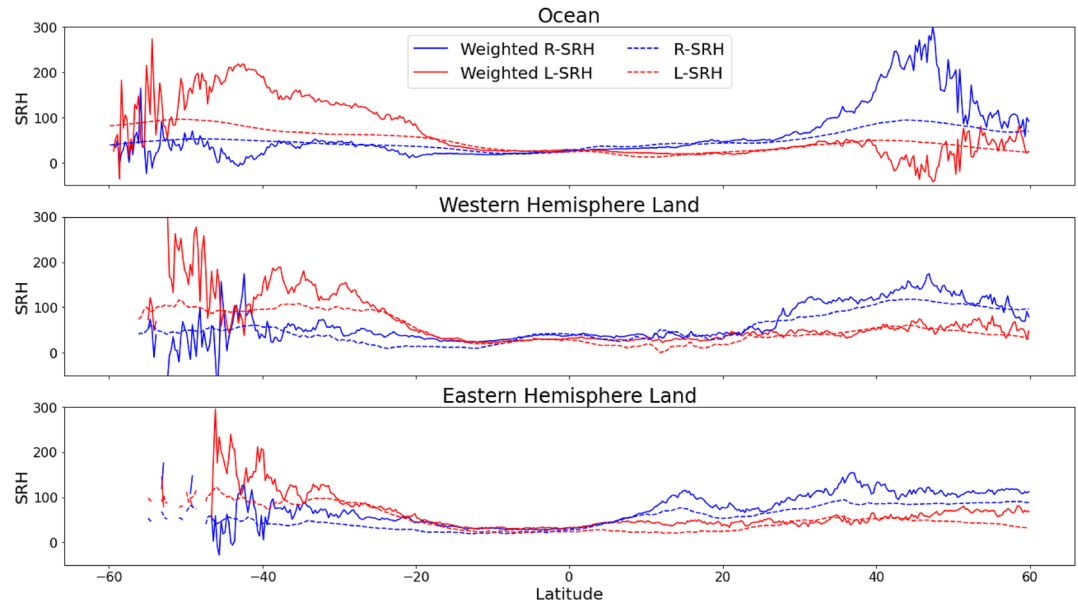


Figure 15. As in Figure 9 but for zonal-mean 0–3 km storm-relative helicity (SRH; $\text{m}^2 \text{s}^{-2}$) for the right-moving (blue) and left-moving (red) storms. Solid lines are weighted by six-hourly $W_{\text{up}} > 10 \text{ m s}^{-1}$ counts in quarter-degree grid bins; dashed lines are the unweighted means. Negative L-SRH (favoring the left-mover) is plotted as positive values. The very large values of the weighted-mean SRH in the subpolar oceans come from a relatively small number of convective events.

4. Conclusions

We have described the global properties of rotating convection in the X-SHiELD global storm resolving model as characterized by 2–5 km updraft helicity (UH). We have shown that UH is a simple and broadly applicable way to characterize the rotation of a wide range of convective updrafts, beyond the original severe supercell thunderstorms it was designed for. The frequencies of intense convection (6-hr maximum updraft velocities of 10 m s^{-1} or greater) match the expected spatial and seasonal distributions, giving credence to the validity of our results. This is further borne out by the direct validation of precipitation and environmental parameters for convection and shear. In all regions cyclonically rotating updrafts (counterclockwise in the northern hemisphere and clockwise in the southern) predominate over anticyclonic updrafts, a preference stronger over higher latitudes especially in the ocean. In the deep tropics there is a near equality in the counts of cyclonic and anticyclonic updrafts, with the ratio between cyclonic and anticyclonic increasing poleward until about 20° latitude, leveling off at higher latitudes. This is complicated over the continents by the more complex geography, and several continental convective hot spots are present in which anticyclonic updrafts are not uncommon. Cyclonic rotation is still preferred nearly everywhere, a preference that only increases at higher UH thresholds.

An examination of marine convection over the western Pacific reveals that the rotating updrafts are individual convective cells. Cyclonic storms predominate in the subtropics while there is near equality in the deep tropics, where many updrafts may not rotate at all. These individual thunderstorms are not sufficiently long-lived (at most a few hours) for planetary vorticity to directly affect storm formation, so we conclude that the synoptic-scale environment is likely the determining factor. There is a correspondence with the convection-weighted storm-relative helicity (SRH) of the appropriate sign and of the number of rotating storms in these regions, indicating that some of the difference can be explained by environmental shear. X-SHiELD also produces numerous pairs of counter-rotating storms, indicating that we are not merely seeing the convergence of environmental relative vorticity into updrafts. We conclude that, similarly to the well-understood process leading to the origin of rotation in continental storms, the relative prevalence of cyclonic to anticyclonic storms arises from the ambient SRH in the synoptic environment for cyclonic storms (right-moving in the northern hemisphere) compared to that for anticyclonic storms. The synoptic systems in which the storms are embedded are long-lived enough to be affected by the planetary rotation, which will prefer one sign of environmental rotation at higher latitudes. This does not however rule out the appearance of either sense of updraft rotation for individual events. The analogy to mid-latitude continental convection should also not be taken too far as it is recognized that while some of the

same processes may be at work (Hogsett & Stewart, 2014) the environments tend to be very different (Kilroy & Smith, 2015). Given the wide range of processes that can give rise to a rotating updraft (baroclinic generation, barotropic shearing, convergence of environmental vorticity, tilting of environmental shear, etc.) and the global scope of this survey, we have left conclusive determinations of which processes are active in which regions to future research.

This explanation does not consider the regional factors which complicate the pattern, especially over the mid-latitude continental hot spots in which the preference for one sign of rotation is much less pronounced. Some of this variation can be explained by the year-mean pattern of SRH, but there are areas especially in the continental sub-tropics where the preference for cyclonic updrafts is not associated with larger values of cyclonic SRH. One shortcoming of the current version of X-SHIELD is that convection may be over-intense, especially over the oceans where the model produces as much intense convection as is seen over the continents. Since intense convection is rarely seen over the ocean (Houze et al., 2015; Liu et al., 2007; Takahashi et al., 2023) this could point to some distinctive property of tropical convection the model is not yet picking up on, or shortcomings in the modeled microphysics or planetary boundary layer scheme. One challenge with GSRMs is that explicit convection cannot be “tuned” as is done with parameterized convection (Hourdin et al., 2017) and so producing convective statistics and upscale impacts to match those in the real atmosphere is more difficult. Another potential limitation of our results is that the evolution of counter-rotating pairs of storms is heavily dependent on specifics of cold pool structure (Grasso, 2000), which in turn depends on the details of the microphysics and boundary layer schemes. This is illustrated by our results in the central plains of the United States, in which the model simulates a nearly equal number of cyclonic and anticyclonic updrafts for the weaker $50 \text{ m}^2 \text{ s}^{-2}$ threshold (Figure 3). This is despite the well-understood predominance of cyclonic rotation in severe convection, a distinction which is simulated by X-SHIELD (Figures 5 and 7). Other mechanisms for creating local rotation, including convergence of vertical or horizontal vorticity (Nolan, 2011) and the creation of shear zones, may also be at work. The potential model dependence on updraft frequency, intensity, and rotation is a source of uncertainty in these results; Dauhut and Hohenegger (2022) came to a similar conclusion in their study of stratospheric hydration in a GSRM.

Future work could establish whether rotating updrafts have a broader significance in the earth system, including whether rotating updrafts are longer-lived worldwide. This could have significant implications for storm impacts and on the larger-scale impacts of intense convection. Regional seasonal variations in the two senses of UH (Northeastern Pacific, Gulf of Mexico, India) are of additional interest. The seasonal variation in severe weather events in the Southeastern US is well-studied (Ashley, 2007; Brooks et al., 2003; Childs et al., 2018) and has a notable late-season secondary maximum in severe weather, and other areas may be of equal scientific and societal interest. GSRMs like X-SHIELD provide a new way to extend the traditional focus of rotating convection beyond severe continental convection and to give a broader view of the significance of this phenomenon, including how rotating convection may change in a warmer climate.

Data Availability Statement

Public releases of SHIELD are available at https://github.com/NOAA-GFDL/SHIELD_build. The code used for the version of X-SHIELD in this paper is available in Harris, Zhou, Chen, et al. (2022). Data used to produce the figures is available in Harris, Zhou, Kaltenbaugh, et al. (2022). GPM data in Figure 6 are from Huffman et al. (2019). Tornado events in Figure 8b are from the Storm Events Database at <https://www.ncdc.noaa.gov/stormevents>.

References

- Ashley, W. S. (2007). Spatial and temporal analysis of tornado fatalities in the United States: 1880–2005. *Weather and Forecasting*, 22, 1214–1228. <https://doi.org/10.1175/2007waf2007004.1>
- Bechtold, P., Semane, N., Lopez, P., Chaboureau, J., Beljaars, A., & Bormann, N. (2014). Representing equilibrium and nonequilibrium convection in large-scale models. *Journal of the Atmospheric Sciences*, 71(2), 734–753. <https://doi.org/10.1175/jas-d-13-0163.1>
- Becker, T., Bechtold, P., & Sandu, I. (2021). Characteristics of convective precipitation over tropical Africa in storm-resolving global simulations. *Quarterly Journal of the Royal Meteorological Society*, 147(741), 4388–4407. <https://doi.org/10.1002/qj.4185>
- Boucher, O., Servonnat, J., Albright, A. L., Aumont, O., Balkanski, Y., Bastrikov, V., et al. (2020). Presentation and evaluation of the IPSL-CM6A-LR climate model. *Journal of Advances in Modeling Earth Systems*, 12, e2019MS002010. <https://doi.org/10.1029/2019MS002010>
- Brooks, H. E., Doswell, C. A., III, & Kay, M. P. (2003). Climatological estimates of local daily tornado probability for the United States. *Weather and Forecasting*, 18, 626–640. [https://doi.org/10.1175/1520-0434\(2003\)018<0626:ceoldt>2.0.co;2](https://doi.org/10.1175/1520-0434(2003)018<0626:ceoldt>2.0.co;2)
- Bunkers, M. J. (2002). Vertical wind shear associated with left-moving supercells. *Weather and Forecasting*, 17(4), 845–855. [https://doi.org/10.1175/1520-0434\(2002\)017<0845:vvsawl>2.0.co;2](https://doi.org/10.1175/1520-0434(2002)017<0845:vvsawl>2.0.co;2)

Acknowledgments

The authors thank Jong-Il Han at the Environmental Modeling Center (EMC) for providing and assisting with the latest version of the TKE-EDMF scheme, and George Gayno and Helin Wei also of EMC for assistance with high-resolution land model inputs. Daniel Klocke (Max Planck Institute for Meteorology) provided ECMWF analyzed SSTs. Ming Zhao and Stephen Garner (GFDL) provided insightful reviews materially improving this paper. Stephan Fueglistaler (Princeton University) encouraged this year-long simulation and both GFDL and CIMES management facilitated this project. Finally, the authors acknowledge S-J Lin's leadership in creating FV3 and the GSRM predecessors to X-SHIELD, and his generational talent and vision that led to the success of these models. The authors thank the editor, Robert Rogers, and three anonymous reviewers whose reviews led to material improvements in this manuscript. Zhou and Cheng are supported under awards NA18OAR4320123, NA19OAR0220146, and NA19OAR0220147 from the National Oceanic and Atmospheric Administration (NOAA), U.S. Department of Commerce. Cheng's contributions are additionally supported by the Weather Program Office, Office of Oceanic and Atmospheric Research, NOAA, and the NOAA Research Global-Nest Initiative. Bretherton and Clark were supported by the Allen Institute for Artificial Intelligence. The statements, findings, conclusions, and recommendations are those of the authors and do not necessarily reflect the views of NOAA, or the U.S. Department of Commerce.

- Bunkers, M. J., Klimowski, B. A., Zeitler, J. W., Thompson, R. L., & Weisman, M. L. (2000). Predicting supercell motion using a new hodograph technique. *Weather and Forecasting*, *15*(1), 61–79. [https://doi.org/10.1175/1520-0434\(2000\)015<0061:psmuan>2.0.co;2](https://doi.org/10.1175/1520-0434(2000)015<0061:psmuan>2.0.co;2)
- Cheng, K.-Y., Harris, L., Bretherton, C., Merlis, T. M., Bolot, M., Zhou, L., et al. (2022). Impact of warmer sea surface temperature on the global pattern of intense convection: Insights from a global storm resolving model. *Geophysical Research Letters*, *49*, e2022GL099796. <https://doi.org/10.1029/2022GL099796>
- Childs, S. J., Schumacher, R. S., & Allen, J. T. (2018). Cold-season tornadoes: Climatological and meteorological insights. *Weather and Forecasting*, *33*, 671–691. <https://doi.org/10.1175/waf-d-17-0120.1>
- Dauhut, T., & Hohenegger, C. (2022). The contribution of convection to the stratospheric water vapor: The first budget using a global storm-resolving model. *Journal of Geophysical Research: Atmospheres*, *127*, e2021JD036295. <https://doi.org/10.1029/2021JD036295>
- Davies-Jones, R. P. (1984). Streamwise vorticity: The origin of updraft rotation in supercell storms. *Journal of the Atmospheric Sciences*, *41*, 2991–3006. [https://doi.org/10.1175/1520-0469\(1984\)041<2991:svtoou>2.0.co;2](https://doi.org/10.1175/1520-0469(1984)041<2991:svtoou>2.0.co;2)
- Droegemeier, K. K., Lazarus, S. M., & Davies-Jones, R. P. (1993). The influence of helicity on numerically simulated convective storms. *Monthly Weather Review*, *121*, 2005–2029. [https://doi.org/10.1175/1520-0493\(1993\)121<2005:tiohon>2.0.co;2](https://doi.org/10.1175/1520-0493(1993)121<2005:tiohon>2.0.co;2)
- Duras, J., Ziemann, F., & Klocke, D. (2021). The diamond winter data collection. *EGU21*. <https://doi.org/10.5194/egusphere-egu21-4687>
- Emanuel, K. A. (1989). Dynamical theories of tropical convection. *Australian Meteorological Magazine*, *37*(1).
- Gehne, M., Hamill, T. M., Kiladis, G. N., & Trenberth, K. E. (2016). Comparison of global precipitation estimates across a range of temporal and spatial scales. *Journal of Climate*, *29*(21), 7773–7795. <https://doi.org/10.1175/jcli-d-15-0618.1>
- Grasso, L. D. (2000). The dissipation of a left-moving cell in a severe storm environment. *Monthly Weather Review*, *128*(8), 2797–2815. [https://doi.org/10.1175/1520-0493\(2000\)128<2797:doalm>2.0.co;2](https://doi.org/10.1175/1520-0493(2000)128<2797:doalm>2.0.co;2)
- Guimond, S. R., Heymsfield, G. M., & Turk, F. J. (2010). Multiscale observations of hurricane dennis (2005): The effects of hot towers on rapid intensification. *Journal of the Atmospheric Sciences*, *67*(3), 633–654. <https://doi.org/10.1175/2009JAS3119.1>
- Han, J., & Bretherton, C. S. (2019). TKE-based moist eddy-diffusivity mass-flux (EDMF) parameterization for vertical turbulent mixing. *Weather and Forecasting*, *34*(4), 869–886. <https://doi.org/10.1175/WAF-D-18-0146.1>
- Han, J., Wittek, M. L., Teixeira, J., Sun, R., Pan, H.-L., Fletcher, J. K., & Bretherton, C. S. (2016). Implementation in the NCEP GFS of a hybrid eddy-diffusivity mass-flux (EDMF) boundary layer parameterization with dissipative heating and modified stable boundary layer mixing. *Weather and Forecasting*, *31*(1), 341–352. <https://doi.org/10.1175/WAF-D-15-0053.1>
- Harris, L., Zhou, L., Chen, J.-H., Gao, K., Tong, M., Cheng, K.-Y., & Clark, S. (2022). SHIELD_PIRE_production_202103 (PIRE_production_202103). [Software]. Zenodo. <https://doi.org/10.5281/zenodo.6941034>
- Harris, L., Zhou, L., Kaltenbaugh, A., Clark, S., Cheng, K.-Y., & Bretherton, C. (2022). Datasets supporting the original submission of Harris et al. "A global survey of rotating convective updrafts in the GFDL X-SHIELD 2021 global storm resolving model" (1.0) [Dataset]. Zenodo. <https://doi.org/10.5281/zenodo.6949403>
- Harris, L., Zhou, L., Lin, S.-J., Chen, J.-H., Chen, X., Gao, K., et al. (2020). GFDL SHIELD: A unified system for weather-to-seasonal prediction. *Journal of Advances in Modeling Earth Systems*, *12*, e2020MS002223. <https://doi.org/10.1029/2020MS002223>
- Hendricks, E. A., Montgomery, M. T., & Davis, C. A. (2004). The role of “vortical” hot towers in the formation of tropical cyclone diana (1984). *Journal of the Atmospheric Sciences*, *61*(11), 1209–1232. [https://doi.org/10.1175/1520-0469\(2004\)061<1209:trovht>2.0.co;2](https://doi.org/10.1175/1520-0469(2004)061<1209:trovht>2.0.co;2)
- Herman, G. R., Nielsen, E. R., & Schumacher, R. S. (2018). Probabilistic verification of storm prediction center convective outlooks. *Weather and Forecasting*, *33*, 161–184. <https://doi.org/10.1175/waf-d-17-0104.1>
- Hersbach, H., Bell, B., Berrisford, P., Hirahara, S., Horányi, A., Muñoz-Sabater, J., et al. (2020). The ERA5 global reanalysis. *Quarterly Journal of the Royal Meteorological Society*, *146*, 1999–2049. <https://doi.org/10.1002/qj.3803>
- Hitchens, N. M., Brooks, H. E., & Kay, M. P. (2013). Objective limits on forecasting skill of rare events. *Weather and Forecasting*, *28*(2), 525–534. <https://doi.org/10.1175/WAF-D-12-00113.1>
- Hogsett, W. A., & Stewart, S. R. (2014). Dynamics of tropical cyclone intensification: Deep convective cyclonic “left movers”. *Journal of the Atmospheric Sciences*, *71*(1), 226–242. <https://doi.org/10.1175/jas-d-12-0284.1>
- Hourdin, F., Mauritsen, T., Gettelman, A., Golaz, J., Balaji, V., Duan, Q., et al. (2017). The art and science of climate model tuning. *Bulletin of the American Meteorological Society*, *98*(3), 589–602. <https://doi.org/10.1175/bams-d-15-00135.1>
- Houze, R. A., Jr., Rasmussen, K. L., Zuluaga, M. D., & Brodzik, S. R. (2015). The variable nature of convection in the tropics and subtropics: A legacy of 16 years of the tropical rainfall measuring mission satellite. *Reviews of Geophysics*, *53*(3), 994–1021. <https://doi.org/10.1002/2015RG000488>
- Houze, R. A., Jr., Wilton, D. C., & Smull, B. F. (2007). Monsoon convection in the himalayan region as seen by the TRMM precipitation radar. *Quarterly Journal of the Royal Meteorological Society*, *133*, 1389–1411. <https://doi.org/10.1002/qj.106>
- Huffman, G. J., Stocker, E. F., Bolvin, D. T., Nelkin, E. J., & Tan, J. (2019). GPM IMERG final precipitation L3 half hourly 0.1 degree x 0.1 degree V06 [Dataset]. Goddard Earth Sciences Data and Information Services Center. <https://doi.org/10.5067/GPM/IMERG/3B-HH/06>
- Judt, F., Klocke, D., Rios-Berrios, R., Vanniere, B., Ziemann, F., Auger, L., et al. (2021). Tropical cyclones in global storm-resolving models. *Journal of the Meteorological Society of Japan*, *99*, 579–602. <https://doi.org/10.2151/jmsj.2021-029>
- Kain, J. S., Weiss, S. J., Bright, D. R., Baldwin, M. E., Levit, J. J., Carbin, G. W., et al. (2008). Some practical considerations regarding horizontal resolution in the first generation of operational convection-allowing NWP. *Weather and Forecasting*, *23*(5), 931–952. <https://doi.org/10.1175/waf2007106.1>
- Kilroy, G. (2021). Evolution of convective characteristics during tropical cyclogenesis (2021). *Quarterly Journal of the Royal Meteorological Society*, *147*, 2103–2123. <https://doi.org/10.1002/qj.4011>
- Kilroy, G., & Smith, R. K. (2015). Tropical cyclone convection: The effects of a vortex boundary-layer wind profile on deep convection. *Quarterly Journal of the Royal Meteorological Society*, *141*, 714–726. <https://doi.org/10.1002/qj.2383>
- Lin, S.-J., & Rood, R. (1996). Multidimensional flux-form semi-lagrangian transport schemes. *Monthly Weather Review*, *124*(9), 2046–2070. [https://doi.org/10.1175/1520-0493\(1996\)124<2046:mfslt>2.0.co;2](https://doi.org/10.1175/1520-0493(1996)124<2046:mfslt>2.0.co;2)
- Lin, S.-J., & Rood, R. B. (1997). An explicit flux-form semi-lagrangian shallow-water model on the sphere. *The Quarterly Journal of the Royal Meteorological Society*, *123*, 2477–2498. <https://doi.org/10.1002/qj.49712354416>
- Liu, C., Zipser, E. J., & Nesbitt, S. W. (2007). Global distribution of tropical deep convection: Different perspectives from TRMM infrared and radar data. *Journal of Climate*, *20*(3), 489–503. <https://doi.org/10.1175/JCLI4023.1>
- Markowski, P. M., Straka, J. M., Rasmussen, E. N., & Blanchard, D. O. (1998). Variability of storm-relative helicity during vortex. *Monthly Weather Review*, *126*(11), 2959–2971. [https://doi.org/10.1175/1520-0493\(1998\)126<2959:vosrhd>2.0.co;2](https://doi.org/10.1175/1520-0493(1998)126<2959:vosrhd>2.0.co;2)
- Miyamoto, Y., Kajikawa, Y., Yoshida, R., Yamaura, T., Yashiro, H., & Tomita, H. (2013). Deep moist atmospheric convection in a subkilometer global simulation. *Geophysical Research Letters*, *40*, 4922–4926. <https://doi.org/10.1002/grl.50944>

- Nolan, D. S. (2011). Evaluating environmental favorableness for tropical cyclone development with the method of point-downscaling. *Journal of Advances in Modeling Earth Systems*, 3, M08001. <https://doi.org/10.1029/2011MS000063>
- Nugent, J. M., Turbeville, S. M., Bretherton, C. S., Blossey, P. N., & Ackerman, T. P. (2022). Tropical cirrus in global storm-resolving models: 1. Role of deep convection. *Earth and Space Science*, 9, e2021EA001965. <https://doi.org/10.1029/2021EA001965>
- Potvin, C. K., Carley, J. R., Clark, A. J., Wicker, L. J., Skinner, P. S., Reinhart, A. E., et al. (2019). Systematic comparison of convection-allowing models during the 2017 NOAA HWT spring forecasting experiment. *Weather and Forecasting*, 34(5), 1395–1416. <https://doi.org/10.1175/waf-d-19-0056.1>
- Putman, W. M., & Lin, S. J. (2007). Finite-volume transport on various cubed-sphere grids. *Journal of Computational Physics*, 227(1), 55–78. <https://doi.org/10.1016/j.jcp.2007.07.022>
- Rogers, R. (2010). Convective-scale structure and evolution during a high-resolution simulation of tropical cyclone rapid intensification. *Journal of the Atmospheric Sciences*, 67(1), 44–70. <https://doi.org/10.1175/2009JAS3122.1>
- Romatschke, U., Medina, S., & Houze, R. A., Jr. (2010). Regional, seasonal, and diurnal variations of extreme convection in the south asian region. *Journal of Climate*, 23(2), 419–439. <https://doi.org/10.1175/2009jcli3140.1>
- Satoh, M., Stevens, B., Judt, F., Khairoutdinov, M., Lin, S.-J., Putman, W. M., & Düben, P. (2019). Global cloud-resolving models. *Current Climate Change Reports*, 5(3), 172–184. <https://doi.org/10.1007/s40641-019-00131-0>
- Seiki, T., Roh, W., & Satoh, M. (2022). Cloud microphysics in global cloud resolving models. *Atmosphere-Ocean*, 60(3–4), 477–505. <https://doi.org/10.1080/07055900.2022.2075310>
- Sobash, R. A., Kain, J. S., Bright, D. R., Dean, A. R., Coniglio, M. C., & Weiss, S. J. (2011). Probabilistic forecast guidance for severe thunderstorms based on the identification of extreme phenomena in convection-allowing model forecasts. *Weather and Forecasting*, 26(5), 714–728. <https://doi.org/10.1175/WAF-D-10-05046.1>
- Stephan, C. C., Duras, J., Harris, L., Klocke, D., Putman, W. M., Taylor, M., et al. (2022). Atmospheric energy spectra in global kilometre-scale models. *Tellus A: Dynamic Meteorology and Oceanography*, 74, 280–299. <https://doi.org/10.16993/tellusa.26>
- Stevens, B., Satoh, M., Auger, L., Biercamp, J., Bretherton, C. S., Chen, X., et al. (2019). Dyamond: The dynamics of the atmospheric general circulation modeled on non-hydrostatic domains. *Progress in Earth and Planetary Science*, 6, 61. <https://doi.org/10.1186/s40645-019-0304-z>
- Takahashi, H., Luo, Z. J., Stephens, G., & Mulholland, J. P. (2023). Revisiting the land-ocean contrasts in deep convective cloud intensity using global satellite observations. *Geophysical Research Letters*, 50, e2022GL102089. <https://doi.org/10.1029/2022GL102089>
- Trapp, R. J., Stumpf, G. J., & Manross, K. L. (2005). A reassessment of the percentage of tornadic mesocyclones. *Weather and Forecasting*, 20(4), 680–687. <https://doi.org/10.1175/WAF864.1>
- Turbeville, S. M., Nugent, J. M., Ackerman, T. P., Bretherton, C. S., & Blossey, P. N. (2022). Tropical cirrus in global storm-resolving models: 2. Cirrus life cycle and top-of-atmosphere radiative fluxes. *Earth and Space Science*, 9, e2021EA001978. <https://doi.org/10.1029/2021EA001978>
- Verbout, S. M., Brooks, H. E., Leslie, L. M., & Schultz, D. M. (2006). Evolution of the U.S. Tornado Database: 1954–2003. *Weather and Forecasting*, 21(1), 86–93.
- Wang, Z. (2018). What is the key feature of convection leading up to tropical cyclone formation? *Journal of the Atmospheric Sciences*, 75(5), 1609–1629. <https://doi.org/10.1175/jas-d-17-0131.1>
- Wedi, N. P., Polichtchouk, I., Dueben, P., Anantharaj, V. G., Bauer, P., Boussetta, S., et al. (2020). A baseline for global weather and climate simulations at 1 km resolution. *Journal of Advances in Modeling Earth Systems*, 12, e2020MS002192. <https://doi.org/10.1029/2020MS002192>
- Zawislak, J. (2020). Global survey of precipitation properties observed during tropical cyclogenesis and their differences compared to nondeveloping disturbances. *Monthly Weather Review*, 148(4), 1585–1606. <https://doi.org/10.1175/MWR-D-18-0407.1>
- Zhao, M., Golaz, J.-C., Held, I. M., Guo, H., Balaji, V., Benson, R., et al. (2018). The GFDL global atmosphere and land model AM4.0/LM4.0: 1. Simulation characteristics with prescribed SSTs. *Journal of Advances in Modeling Earth Systems*, 10, 691–734. <https://doi.org/10.1002/2017MS001208>
- Zhou, L., Harris, L., Chen, J.-H., Gao, K., Guo, H., Xiang, B., et al. (2022). Improving global weather prediction in GFDL SHiELD through an upgraded GFDL cloud microphysics scheme. *Journal of Advances in Modeling Earth Systems*, 14, e2021MS002971. <https://doi.org/10.1029/2021MS002971>
- Zhou, L., Lin, S.-J., Chen, J.-H., Harris, L. M., Chen, X., & Rees, S. L. (2019). Toward convective-scale prediction within the next generation global prediction system. *Bulletin of the American Meteorological Society*, 100, 1225–1243. <https://doi.org/10.1175/BAMS-D-17-0246.1>